Salvino Ciccariello

Dipartimento di Fisica «G. Galilei» e unità INFM.,
via Marzolo 8,
I-35131 Padova, Italy
ciccariello@pd.infn.it

Moments of the density microscopic fluctuation and SAS background contribution

Abstract

Some models of density microscopic fluctuations have been numerically analysed in order to study the behaviour of the related background contribution. The results suggest that this contribution can fairly be described by an even polynomial of the scattering vector whose coefficients are simply related to the moments of the density microscopic fluctuation. In this way the parameter values, determined by a best-fit procedure to account for background contributions in the case of real samples, acquire a well-defined physical meaning. The procedure is applied to the small-angle X-ray intensities relevant to a polymer sample analysed at different temperatures, and yields satisfactory results.

Key words: *Porod's law, density microscopic fluctuation, background contribution, moments.*

1. Introduction

The basic assumption of small-angle scattering (SAS) theory consists in approximating n(r), the scattering density (i.e. the electron density or the scattering-length density depending on whether the ingoing particles are x-rays or neutrons) of the sample, with a discrete-valued function $n_D(r)$ (Debye et al. [1]). In the following we shall restrict ourselves to the case where $n_D(r)$ takes only two values, denoted by n_1 and n_2. In this way, the regions of the sample where $n_D(r)$ is equal to n_1 or to n_2 form the homogeneous phases „1" and „2", respectively. However, $n_D(r)$ only represents an approximation of the true scattering density n(r) of the given sample. Thus, on rigorous grounds, we must write

$$n(r) = n_D(r) + n_D(r) \qquad (1.1)$$

where $v_D(r)$ represents the difference between n(r) and $n_D(r)$. This quantity is called the scattering density of the Debye idealised sample or, more simply, the Debye idealised scattering density, while $v_D(r)$ is the density microscopic fluctuation function with respect to the Debye idealised one. Clearly, $n_D(r)$ must be chosen in such a way that it is as close as possible to n(r). Recently Ciccariello [2] put forth the equations whose solution answers the aforesaid problem. However, this procedure requires the knowledge of n(r) as well as a great deal of mathematical computations, being essentially a matter of trial and error. Thus, on a practical ground, one needs to postulate the existence of $n_D(r)$, and one is confined to finding out some general constraints on the latter, as will become clear later. For the moment, it will be assumed that both n(r) and $n_D(r)$ are known. For a statistically isotropic sample, the observed scattering intensity is

$$I(q) = (1/4\pi)\int |\tilde{n}(q\hat{q})|^2 d\hat{q} \qquad (1.2)$$

where $\tilde{n}(q) = \tilde{n}(q\hat{q})$ is the Fourier transform (FT) of n(r), i.e.

$$\tilde{n}(q) = \int e^{iq\cdot r} n(r) dv \qquad (1.3)$$

and the integral in Eq. (1.2) is performed over all possible directions $\hat{q} \equiv q/q$ of the scattering vector q, whose modulus q is related to the scattering angle θ and to the radiation wave-length λ by the well-known relation $q = (4\pi/\lambda)\sin(\theta/2)$. Then, after Fourier transforming Eq. (1.1) and substituting the result in Eq. (1.2) one finds, as shown by Ciccariello, Goodisman & Brumberger [3], that

$$I(q) = I_D(q) + I_{bck}(q), \qquad (1.4)$$

where

$$I_D(q) \equiv (1/4\pi)\int |\tilde{n}_D(q\hat{q})|^2 d\hat{q} \qquad (1.5)$$

and

$$I_{bck}(q) \S I_{mfl}(q) + I_{int}(q) \qquad (1.6)$$

with

$$I_{mfl}(q) = (1/4\pi)\int |\tilde{v}_D(q\hat{q})|^2 d\hat{q} \qquad (1.7)$$

and

(Equation 1.8)

In Eq. (1.8), $\Re$ and the overbar denote the operations of taking the real part and of complex conjugation, respectively. Eq. (1.4) shows that the scattering intensity observed is the sum of two contributions, $I_D(q)$ and $I_{bck}(q)$. The first represents the intensity which would be observed with a scattering experiment performed on a sample with a scattering density equal to $n_D(r)$, and this will be called the Debye ideal scattering intensity. It is determined only by the geometry of the interface (putting aside the linear dependence on the contrast) and contains all the information, obtainable by a scattering experiment, on the geometrical structure of the sample. This property explains why the knowledge of $I_D(q)$ is physically important. Eq. (1.4) shows that unfortunately $I_D(q)$ cannot be obtained from the observed I(q) because we need to subtract the background contribution $I_{bck}(q)$, which is not directly measurable. This problem is commonly referred to as the background problem, and it is empirically solved as follows. We may employ the property that, in the outer portion of the q-range explored in SAS experiments, $I_D(q)$ has a known analytic expression, essentially given by Porod's law [4] (see also Ref. [5]), namely

$$I_D(q) \approx I_{D,as}(q) = \frac{2\pi\Delta n^2 S}{q^4} \qquad (1.9)$$

where $\Delta n^2 \equiv (n_1 - n_2)^2$ is the contrast and S the area of the interphase surface. Then one assumes [6–12] that in the same q-range, $I_{bck}(q)$ will be well approximated by the sum of the first M terms of its power expansion, i.e.

$$I_{bck}(q) = \sum_{m=0}^{M} b_{2m} q^{2m} \qquad (1.10)$$

and the unknown quantities Δn^2, $b_0,\ldots,b_{2M}$ are determined by best-fitting the observed intensity to the sum of the expressions reported on the right hand

Equation 1.8

$$I_{int}(q) = (1/2\pi)\Re\int \left[\overline{\tilde{n}_D(q\hat{q})}\tilde{v}_D(q\hat{q})\right] d\hat{q} \qquad (1.8)$$

sides (rhs) of Eqs. (1.9) and (1.10). By so doing, $I_{bck}(q)$ is determined throughout the explored q-range, where $I_D(q)$ also turns out to be determined as $I(q)-I_{bck}(q)$. This procedure is clearly a trial and error one, since the aforesaid parameters are determined by requiring that quantity be the smallest one. In Eq. (1.11), ε_j denotes the experimental error on the intensity value $I(q_j)$ relevant to the observed scattering vector q_j, while the sum runs over all the q_j values which lie within the chosen outer q-range, considered to be asymptotic. The best choice of M can be made on the basis of the statistical χ^2-test [13], while the arbitrariness in the choice of the asymptotic q-range can be reduced by requiring that the best-fit results do not change appreciably for different choices of the best-fitted q-range. Even though the procedure is not free of ambiguities, it appears fairly sound on statistical grounds.

However, two questions still remain to be considered:

a) is the procedure sound even when $I_{bck}(q)$ turns out to be larger than $I_D(q)$ in the asymptotic range?
b) do the parameters $b_0,..,b_{2M}$ have a physical meaning?

In a recent paper [14], Sobry & Ciccariello answered these two questions, at least on an empirical basis.

After analysing some models of density microscopic fluctuations, they found that:

- the contribution $I_{int}(q)$ is generally negligible in comparison to $I_{mfl}(q)$ in the (SAS) explored q-range;
- the analysis makes sense even when $I_{bck}(q)$ is one order of magnitude larger than $I_{D,as}(q)$;
- $I_{bck}(q)$ can be approximated by the first M terms of the power series expansion of $I_{mfl}(q)$;
- the coefficients of this expansion are the moments of the auto-correlation function of the density microscopic fluctuation;
- assuming that density microscopic fluctuation is isotropic, the aforesaid coefficients are simply related to its moments.

We stress that these conclusions have an important practical relevance, particularly when one tries to extract numerical information on the interface areas for a set of samples at different physical conditions. The application of Porod's law makes it unavoidable, in practice, to subtract the appropriate background contributions by carrying through the numerical procedure reported above. In this way, the resulting best-fitted parameters, which determine the background contributions, can be immediately related to the moments of the density microscopic fluctuations, and one can infer how the latter change as the physical conditions of the sample vary.

The aim of this paper is to report on the previous results while adding some original details which were anticipated in [14]. The plan of the paper is as follows. Section 2 is devoted to a more thorough discussion of the Debye idealisation, so as to understand more easily the reasons why, in the SAS outer q-range, $I_D(q)$ is well approximated by its leading asymptotic term while $I_{bck}(q)$ is fairly described by the first terms of the power expansion of $I_{mfl}(q)$. Besides, it also reports the general mathematical relations. Section 3 illustrates the numerical results obtained by considering a fluid-like model for the density microscopic fluctuation. Section 4 reports on a practical application to a polymer sample, analysed at different temperatures. Finally, section 5 contains the concluding remarks.

Equation 1.11

$$\chi^2_M \equiv \sum_{j=N_1}^{N_2} \left[I(q_j) - \left[I_{D,as}(q_j) + I_{bck}(q_j) \right] \right]^2 / \varepsilon_j^2 \qquad (1.11)$$

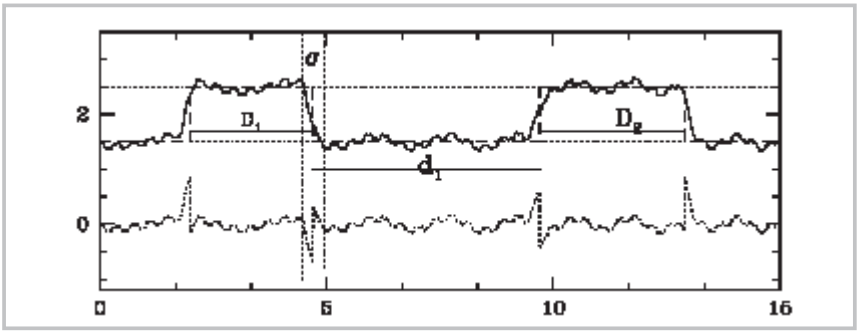

Figure 1. *- In the upper part, the continuous curve shows the density profile for a 1D sample, and the broken line a possible Debye idealisation. In the lower part, the dotted curve is the profile of the resulting density microscopic fluctuation. D_1 and D_2 are the sizes of the two homogeneous particles, and d_1 the distance between the latter. The two vertical dotted lines delimit a diffuse interface region with thickness σ.*

2. Theoretical formulation

As already mentioned, SAS theory assumes that n(r) can be approximated by $n_D(r)$. Figure 1 should help us in better understanding the subtleties of this approximation, as well the conditions to be fulfilled for its validity. In the figure, the continuous line shows the scattering density profile of a 'real' one-dimensional (1D) sample, and the broken linear segments the profile of a possible Debye idealisation. In drawing these segments, we must choose the values of n_1 and n_2, which determine the upper and lower horizontal dotted lines, and we must draw the vertical segments between these two lines. The figure makes it evident that the ambiguity in the choice of n_1 and n_2 is much smaller than that in the drawing of the vertical segments. Each of these can be arbitrarily drawn inside each region where n(x) varies from n_1 to n_2 (or vice versa). The dotted vertical lines delimit one of these regions corresponding to the diffuse interfaces in the case of 3D samples. It is stressed that, while n(r) is a continuous function, both $n_D(r)$ and $\nu_D(r)$ show, at the same points, first-order discontinuities of opposite signs in order that their sum may reproduce the continuous n(r). Moreover, $\nu_D(r)$ is everywhere rather close to zero, except within the diffuse interface regions where it shows discontinuities equal to $\pm(n_1 - n_2)$. However, this rather large variation occurs within segments with size $\bar{\sigma}$, the typical thickness of the diffuse interfaces. By $\bar{D}$ and $\bar{d}$ we denote the typical size of the particles (i.e. D_1 and D_2 in the figure) and the typical distance between the particle boundaries (d_1 in the figure). The Debye idealisation is possible, and almost unique if the ambiguity in the choice of n_1 and n_2 is rather small and if $\bar{\sigma} << \min\left(\bar{D}, \bar{d}\right)$. Clearly, these conditions also hold true in the case of 3D samples, and in the following we shall restrict ourselves to those samples where the aforesaid conditions are met[1].

We must now analyse the asymptotic behaviours, at large q values, of I(q), $I_D(q)$, $I_{mfl}(q)$ and $I_{int}(q)$. As discussed in [3] (see, in particular, Appendix A), the presence of first-order discontinuities in the scattering density is the only phenomenon responsible for the asymptotic behaviour q^{-4} of the scattering intensity.

[1] It is mentioned that for some samples it is not accurate to look at the interface as fixed surfaces owing to possible fluctuations of the latter. This problem is discussed in [15] and [16]. In this paper, we confine ourselves to those samples where these fluctuations are negligible.

If the scattering density is continuous, the scattering intensity asymptotically decreases more quickly than q^{-4}. In other words, it decreases as $q^{-\alpha}$ with $\alpha>4$. Thus, asymptotically, one finds that $I(q)=O(q^{-\alpha})$ with $\alpha>4$, while both $I_D(q)$ and $I_{mfl}(q)$ have the same asymptotic behaviour, i.e.

$$I_D(q) \approx I_{mfl}(q) \approx 2\pi\Delta n^2 S/q^{-4}, \quad (2.1)$$

because, as noted above, both $n_D(r)$ and $\nu_D(r)$ have the same first-order discontinuities aside from the opposite sign factor, which is washed out by the fact that in Eq.(2.1) the value of the first–order discontinuity is squared. From these results and Eqs. (1.4) and (1.6) it follows that the leading asymptotic term of $I_{int}(q)$ is

$$I_{int}(q) \approx -4\pi\Delta n^2 S/q^{-4}, \quad (2.2)$$

since this is the only possibility ensuring an asymptotic decrease faster than q^{-4} for I(q). Despite the fact that $I_D(q)$, $I_{mfl}(q)$ and $I_{mfl}(q)$ and $I_{int}(q)$ have the same q^{-4} asymptotic decrease, the q–range where the asymptotic behaviour occurs is not the same in these three cases. To understand this point, which is extremely important for the following analysis, we refer again to the 1D case shown in Figure 1. From this figure it appears clear that once the spatial resolution is better than min $(\overline{D},\overline{d})$ all the details, in particular the discontinuities, of $n_D(r)$ are observable. This condition amounts to having $q\cdot min(\overline{D},\overline{d})>2\pi$. On the other hand, the scattering intensity becomes sensitive to the positions of the discontinuities (and to their squared amplitudes). Thus, it is fairly described by the Porod contribution. One concludes that

$$I_D(q) \approx 2\pi\Delta n^2 S/q^4$$

provided

$$q\cdot\min(\overline{D},\overline{d}) > 2\pi. \quad (2.3a)$$

By applying the same reasoning to $\nu_D(r)$, one finds that the spatial resolution must be at least equal to $\overline{\sigma}$ for the spikes associated to the first-order discontinuities of $\nu_D(r)$ to be resolved. Thus one obtains

$$I_{mfl}(q) \approx 2\pi\Delta n^2 S/q^4$$

provided

$$q\cdot\overline{\sigma} > 2\pi, \quad (2.3b)$$

and then

$$I_{int}(q) \approx -4\pi\Delta n^2 S/q^4$$

provided

$$q\cdot\overline{\sigma} > 2\pi. \quad (2.3c)$$

These equations show that, if $\overline{\sigma} << \min(\overline{D},\overline{d})$, one can find a q-range where Eq. (2.3a) holds true and where Eqs. (2.3b) and (2.3c) do not. To be more specific, we recall that the q-range explored in SAS experiments is [0.001–0.5]Å^{-1}. Then, according to Eq. (2.3a), Porod behaviour can be expected in the outer part of the explored q-range only for those samples where min $(\overline{D},\overline{d})\geq 50$ Å^2. We also recall that for many samples $\overline{\sigma}$ typically amounts to only a few angstroms, so that it is impossible to use Eqs. (2.3b) and (2.3c) in analysing the tail of the observed intensity. Thus, we need to find an approximation for $I_{mfl}(q)$ and $I_{int}(q)$. To this end, we shall first remark some general properties of these two quantities. From Eq. (1.7) it appears evident that $I_{mfl}(q)$ represents the intensity scattered by a sample with a scattering density equal to $\nu_D(r)$. Hence, it is always non-negative. By contrast, Eq. (1.8) shows that $I_{int}(q)$ depends both on $n_D(r)$ and $\nu_D(r)$. Therefore, it must be considered a genuine interference contribution. It can be negative or positive depending on the considered q-value and, according to Eq. (2.2), it becomes definitely negative as q becomes very large. Following Debye & Bueche [19], we now introduce the so-called scattering density fluctuation of the real and the Debye idealised samples, respectively defined as

$$\eta(r) \equiv n(r)-\langle n\rangle = n(r)-(1/V)\int_V n(r)dv, \quad (2.4a)$$

$$\eta_D(r) \equiv n_D(r)-\langle n_D\rangle = n_D(r)-(1/V)\int_V n_D(r)dv. \quad (2.4b)$$

We have already noted the rather large ambiguity in drawing the geometrical interface, required for defining $n_D(r)$. Hence, we shall assume that the interface drawing can be made in a way such as to ensure that

$$\int_V n(r)\,dv = \int_V n_D(r)\,dv. \quad (2.5)$$

This relation has two consequences. Firstly $\langle n\rangle = \langle n_D\rangle$, and thus

$$\nu_D(r) = n(r)-n_D(r) = \eta(r)-\eta_D(r). \quad (2.6)$$

Secondly,

$$\int \nu_D(r)\,dv = 0 \quad (2.7)$$

which implies that the value of the FT of $\nu_D(r)$ is equal to zero at q = 0, i.e. $\tilde{\nu}_D(0)=0$. Moreover, one can write

$$I(q) = (1/4\pi)\int|\tilde{\eta}(q\hat{q})|^2 d\hat{q} \quad (2.8a)$$

$$I_D(q) = (1/4\pi)\int|\tilde{\eta}_D(q\hat{q})|^2 d\hat{q} \quad (2.8b)$$

and

$$I_{int}(q) = (1/2\pi)\Re\int[\tilde{\eta}_D(q\hat{q})\tilde{\nu}_D(q\hat{q})]d\hat{q} \quad (2.8c)$$

since these expressions coincide with Eqs. (1.2), (1.5) and (1.8), provided $q\neq 0$. In fact, they differ for a δ-like contribution set at the reciprocal space origin when the sample volume becomes infinitely large [20]. Moreover, in this limit the scattering intensities become extensive as it appears evident from the following relations

$$I(q) = V\langle\eta^2\rangle\int e^{iq\cdot r}\gamma(r)dv, \quad (2.9a)$$

$$I_D(q) = V\langle\eta_D^2\rangle\int e^{iq\cdot r}\gamma_D(r)dv, \quad (2.9b)$$

$$I_{mfl}(q) = V\langle\nu_D^2\rangle\int e^{iq\cdot r}\gamma_{mfl}(r)dv, \quad (2.9c)$$

whare (Eq. 2.10)

with $\hat{\omega} = r/r$ and

$$\langle\eta^2\rangle \equiv (1/V)\int\eta^2(r)dv, \quad (2.11)$$

$\langle\eta_D^2\rangle$ and $\langle\nu_D^2\rangle$ being similarly defined. The last three quantities are the mean square fluctuations of the given sample, of the Debye idealised sample and of the sample with scattering density equal to the density microscopic fluctuations, while $\gamma(r)$, $\gamma_D(r)$ and $\gamma_{mfl}(r)$ are the corresponding auto-correlation functions. Comparing Eqs. (2.9a) with (2.8a), (2.9b) with (2.8b) and (2.9c) with (2.8c), one concludes that $\tilde{\eta}(q)/\sqrt{V}$, $\tilde{\eta}_D(q)/\sqrt{V}$ and $\tilde{\nu}_D(q)/\sqrt{V}$ approach finite limits as $V\to\infty$.

Equation 2.10

$$\gamma(r) \equiv (4\pi V\langle\eta^2\rangle)^{-1}\int d\hat{\omega}\int\eta(r_1)\eta(r\hat{\omega}+r_1)dv_1 \quad (2.10a)$$

$$\gamma_D(r) \equiv (4\pi V\langle\eta_D^2\rangle)^{-1}\int d\hat{\omega}\int\eta_D(r_1)\eta_D(r\hat{\omega}+r_1)dv_1 \quad (2.10b)$$

and

$$\gamma_{mfl}(r) \equiv (4\pi V\langle\nu_D^2\rangle)^{-1}\int d\hat{\omega}\int\nu_D(r_1)\nu_D(r\hat{\omega}+r_1)dv_1 \quad (2.10c)$$

[2] This condition is not obeyed by fractal samples, which are characterised by the property that their intensities behave as $q^{-\alpha}$ with $3\leq\alpha<4$ in most of the explored q-range [17,18].

As discussed above, for our class of samples, $I_D(q)$ is well approximated by its asymptotic leading term in the outer portion of the explored q-range, while for $I_{mfl}(q)$ and $I_{int}(q)$ we cannot use the asymptotic expressions (2.3b) and (2.3c) because $q\bar{\sigma} << 2\pi$. Hence, it appears reasonable to expand $\nu_D(q)$ as a power series of q and to approximate $\nu_D(q)$ with the sum of the first terms of this expansion. If we perform this operation directly on Eq. (2.9c) we find that (Eq. 2.12)

where

$$\gamma_{mfl,2j} \equiv (1/(2j+1)!)\int r^{2j}\gamma_{mfl}(r)dv \qquad (2.13)$$

represents the 2jth moment of the autocorrelation function $\gamma_{mfl}(r)$. However, we can also assume that the density microscopic fluctuation is fairly isotropic in the limit $V\to\infty$, so as to have $\nu_D(r)=\nu_D(r)$ and $\tilde{\nu}_D(q) = \tilde{\nu}_D(q)$. In this case, one has (Eq. 2.14)

with (Eq. 2.15)

equal to the 2jth moment of the density microscopic fluctuation. Using Eq. (1.7) one finds that (Eq. 2.16).

The comparison of this equation with Eq. (2.12) shows that the moments of $\gamma_{mfl}(r)$ are simply related to the moments of the density microscopic fluctuation when this is isotropic. Moreover, assuming the validity of condition (2.7), Eq. (2.16) becomes

$$I_{mfl}(q) \approx Vq^4\left[\nu_2 - \nu_4 q^2 + \nu_6 q^4 + \ldots\right]^2, \qquad (2.17)$$

which implies that $\gamma_{mfl,0} = \gamma_{mfl,2} = 0$.

We still need an analytic approximation of $I_{int}(q)$ to obtain an approximation of $I_{bck}(q)$ valid in the non-asymptotic region of $I_{bck}(q)$. Unfortunately this cannot be obtained from Eq. (2.8c) because $I_{inf}(q)$ depends both $\tilde{\nu}_D(q)$ on and on $\tilde{\eta}_D(q)$. Besides, as was noted in the paragraph above, Eq. (2.4a), $I_{int}(q)$, in contrast with $I_{mfl}(q)$, can be positive or negative depending on the q range considered. Recalling Ruland's analysis [7] (see also [10,21] as well as Appendix D of [3]), $I_{int}(q)$ is expected to be the dominant contribution to $I_{bck}(q)$ when the density microscopic fluctuations occur mainly at the borders of the homogeneous phases and are negligible inside the latter. Thus, one expects that $I_{int}(q)$ can be neglected inside the SAS q-range when $\bar{\sigma}$ is very small. As will be reported in the next section, this result was confirmed by the numerical computations of $I_{int}(q)$ for some models of the density microscopic fluctuation.

In conclusion, if the density microscopic fluctuations are mainly internal to the homogeneous phase[3], one finds that $I_{bck}(q) \approx I_{mfl}(q)$ and the latter's expression is given by Eq. (2.12). Moreover, if the density microscopic fluctuation is assumed to be isotropic, i.e. $\nu_D(r) = \nu_D(r)$, then $I_{bck}(q)$ is given by Eq. (2.16). Finally, if condition (2.7) is also assumed, then $I_{bck}(q)$ is given by Eq. (2.17). In this way, the best–fitted parameters are related to the moments of the auto-correlation $\gamma_{mfl}(r)$ in the first case, to the moments of the density microscopic fluctuation in the second case, and the first of these moments is equal to zero in the third case.

3. Some microfluctuation models

In order to test the relative importance of $I_{mfl}(q)$ and $I_{int}(q)$, we have evaluated the angular average of the scattering intensity relevant to a homogeneous ellipsoidal particle with semiaxes a, b and c (with $a \le b \le c$) plus a microfluctuation density $\nu_D(r)$. For the latter we have considered different analytic expressions, both isotropic and anisotropic. We refer to [14] for their explicit expressions and for more details. For all the cases considered, we found that the contribution of $I_{int}(q)$ is negligible (i.e. less than 10%) compared to that of $I_{mfl}(q)$ in the Porod region. However, the resulting shapes of $I_{bck}(q)$ were never similar to realistic background contributions. In fact, the peaks of the resulting $I_{bck}(q)$s developed rather quickly and were rather narrow. Therefore, we considered a more realistic model for microfluctuation densities, which will now be reported.

As before, a homogeneous ellipsoidal particle, with unit scattering density and axis ratios b/a = 0.5 and c/a = 2, was considered. The particle is at the centre of a spherical region, with volume V and radius R_{max} = 20a, where N_{sp}(=64 000) small spherical particles are also present. The scattering density of each of these spheres has the following profile

$$n_{sp}(r) = \begin{cases} \alpha, & \text{if } r < R_1 \\ -\alpha, & \text{if } R_1 < r < R_0 \end{cases} \qquad (3.1)$$

R_1 is determined in terms of R_0 by the condition that $\langle n_{sp} \rangle = 0$. We chose R_0 = 0.15a and α = 0.073. The positions of the 64 000 spheres were randomly generated requiring the distance between each pair of spheres to be greater than $2R_0$, and that each sphere should lie fully within the sphere of radius R_{max}. About ten more runs were performed in order to ensure that the centre of gravity of the considered set of spheres lay close to the origin, so as to be confident that the resulting configuration is also isotropic. [By this construction, the resulting configuration of the spheres should be a snapshot of a fluid of hard sphere [23] in one of its most likely configurations. For this reason, the resulting model of density microscopic fluctuation was named as a fluid-like model.] In this way, the scattering density of the system is

$$n(r) = n_E(r) + \sum_{j=1}^{N_{sp}} n_{sp}(|r - r_j|) \qquad (3.2)$$

Here r_j denotes the position vector of the centre of the jth sphere, $n_E(r)$ is the scattering density of the homogeneous ellipsoid, and the sum over j represents the microscopic density fluctuation. The Fourier transform of $n_E(r)$ is algebraically known [22], and will be denoted by $\tilde{n}_E(q)$. Thus, the FT of Eq. (3.2) reads

$$\tilde{n}(q) = \tilde{n}_E(q) + \tilde{n}_{sp}(q)\sum_{j=1}^{N_{sp}} e^{iq\cdot r_j}, \qquad (3.3)$$

where $\tilde{n}_{sp}(q)$ is the FT of $n_{sp}(r)$, define by Eq. (3.1), and is algebraically known. Comparing Eq. (3.2) with (1.1), one sees that $n_E(r)$ plays the role of $n_D(r)$ and the remaining sum that of $\nu_D(r)$. Thus $\tilde{n}_E(q) \to \tilde{n}_D(q)$, and

$$\tilde{n}_{sp}(q)\sum_{j=1}^{N_{sp}} e^{iq\cdot r_j} \to \tilde{\nu}_D(q). \qquad (3.4)$$

[3] Actually, this assumption can be relaxed, as shown by remark (b) in the conclusive section.

Equation 2.12, 2.14-2.16

$$I_{mfl}(q) \approx V\langle \nu_D^2 \rangle\left[\gamma_{mfl,0} - \gamma_{mfl,2}q^2 + \gamma_{mfl,4}q^4 + \ldots\right] \qquad (2.12)$$

$$\tilde{\nu}_D(q) \approx \sqrt{V}\left[\nu_0 - \nu_2 q^2 + \nu_4 q^4 - \nu_6 q^6 + \ldots\right] \qquad (2.14)$$

$$\nu_{2j} \equiv (1/\sqrt{V}(2j+1)!)\int r^{2j}\nu_D(r)dv \approx (4\pi/\sqrt{V}(2j+1)!)\int_0^\infty r^{2j+2}\nu_D(r)dr \qquad (2.15)$$

$$I_{mfl}(q) \approx V\left[\nu_0 - \nu_2 q^2 + \nu_4 q^4 - \nu_6 q^6 + \ldots\right]^2, \qquad (2.16)$$

If the chosen configuration of the small spheres really were fully isotropic, $\tilde{\nu}_D(q)$ would show no dependence on the direction of q. In reality we found a slight dependence, but we have checked that this dependence decreases as N_{sp} passes from 4000 to 16 000 and to 64 000. The knowledge of $\tilde{n}_D(q)$ and $\tilde{\nu}_D(q)$ and Eqs. (1.5), (1.6) and (1.7) allowed us to evaluate $I_D(q)$, $I_{mfl}(q)$ and $I_{int}(q)$ by numerically evaluating the angular averages involved. In this case, we also found that contribution $I_{int}(q)$ is negligible compared to $I_{mfl}(q)$.

Figure 2 shows the Porod plot of the resulting $I_{mfl}(q)$. The peak position is related to the mean interparticle distance and lies beyond the SAS q-range, while the noise is a consequence of the fact that the volume is not yet very large. Fig. 3a shows the plot of $\langle S(q)\rangle \equiv \left\langle \left| \sum_{j=1}^{N_{sp}} e^{iq\cdot r_j} \right|^2 \right\rangle$, where the angular brackets denote the angular average. In the limit $V\to\infty$ with N_{sp}/V = const, this quantity should approach the structure function of a hard-sphere fluid. In order to reduce the noise, we have smoothed the previous $\langle S(q)\rangle$ by taking the average over the 10 next neighbouring values. The resulting expression is represented by the dotted curve in Fig. 3b, whereas the broken curve is the plot of the structure function (times N_{sp}), obtained from the Percus-Yevick equation [24], of a hard-sphere fluid with the same particle number density N_{sp}/V. The two curves are satisfactorily close, given the small volume where the calculations have been performed. The moments of $\nu_D(r)$ cannot be obtained from the noised $\langle S(q)\rangle$. They can however be evaluated from the algebraic expression $N_{sp}|\tilde{n}_{sp}(q)|^2 h_{PY}(q)$, where $h_{PY}(q)$ is the FT of the total correlation function in the Percus-Yevick approximation. Fig. 4 shows the Porod plot of the resulting scattering intensity I(q) (triangles), while the Porod plot of the scattering intensity $I_D(q) = \langle |\tilde{n}_E(q)|^2 \rangle$ of the homogeneous ellipsoid is given by the dotted (slightly oscillating) curve.

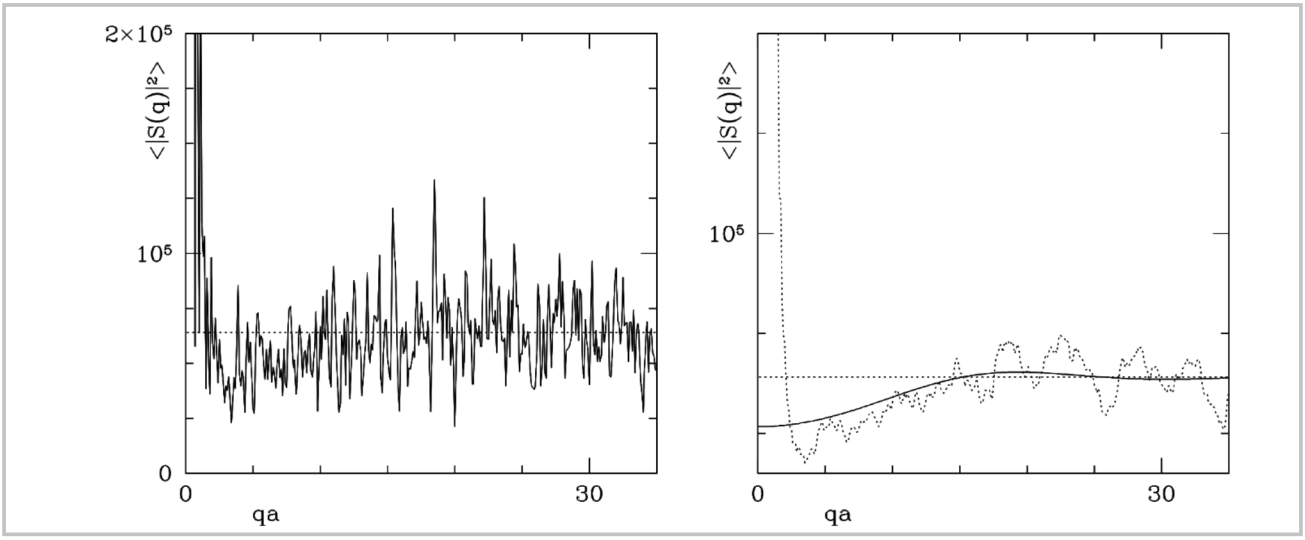

Figure 3. *(a) Plot of the structure function relevant to the considered configuration of spheres; (b) The dotted line represents the smoothing of the result shown on the left by averaging over the 10 next neighbouring values. The broken line is the Percus-Yevick structure function for a hard-sphere liquid with the same particle number density.*

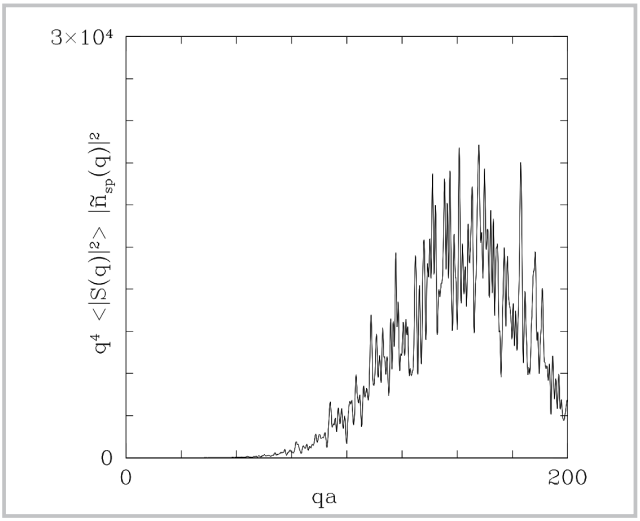

Figure 2. *Porod plot of $I_{mfl}(q)$ for the model of fluid-like density microscopic fluctuation.*

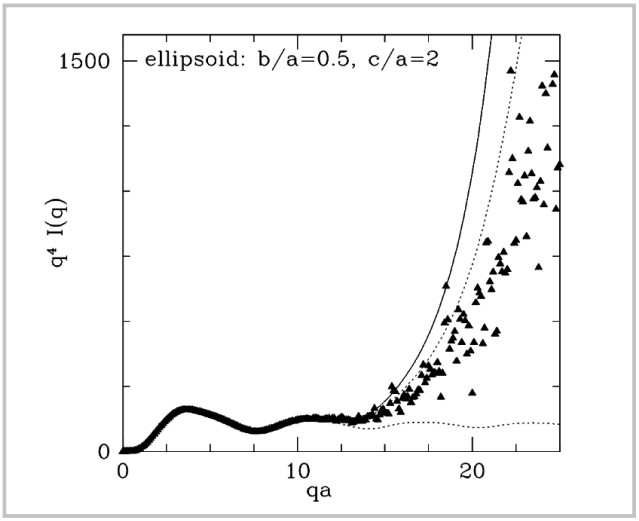

Figure 4. *Porod plot of the total intensity (triangles), of $I_D(q)$ (horizontal dotted line) and of the approximations obtained considering the 2nd (continuous) and 4th moment of the microscopic fluctuation for the model reported in the text.*

The continuous and dotted monotonously increasing curves represent the approximations obtained by considering the scattering intensity of the ellipsoidal particle plus the first or the first two terms of the $I_{mfl}(q)\ q^2$ – power expansion, i.e. $\left(I_D(q)+Vq^4\nu_2^2\right)$ and $\left(I_D(q)+Vq^4\left[\nu_2^2-2\nu_2\nu_4q^2\right]\right)$, respectively. Even though in the two cases the agreement is extremely accurate within the ranges qa < 12,5 and qa < 15, the figure indicates that I(q) can be best-fitted throughout the range qa < 25. In fact, the parameter values of ν_2 and ν_4 obtained in this way are found to deviate less than 20% from the exact ones. This result indicates that positive and rather large deviations from Porod's law can be accounted for by the only contribution (2.17).

4. Numerical analysis of some real intensities

On the basis of the conclusion drawn at the end of the previous section, we have analysed a set of SAS X-ray intensities relevant to a semi-halatotelechelic polymer sample at different temperatures. The sample consists of polystyrene carboxylate of molecular weight 4500 neutralised at one chain end by a mesogenic cation [25]. This compound forms a smectic mesophase in the temperature range [50-150]°C, and has a crystalline structure up to about 50°C. For this reason, the experimental study [26], performed at LURE (Orsay, France), explored the temperature range [40-150]°C. For these samples the determination of the background contribution by Eq. (2.15) looks particularly interesting. In fact, the samples are known to have fairly sharp interfaces, while their chemical composition does not change as their temperatures increase. Hence one should expecte an increase in the microscopic scattering density fluctuation driven by the temperature increase, and this increase should be reflected in the best-fitted values of the moments of $\nu_D(r)$. The intensities were collected with the same experimental set-up with a (Δq)-step of 0.00056 Å^{-1}. They were corrected for absorption and blank, but were not reported to the absolute scale when they were collected. The intensities have been best-fitted in the range [0.05–0.2] Å^{-1} to the analytic expression

$$P_{PD}/q^4+Vq^4\left[\sum_{j=2}^{M}(-1)^j\nu_{2j}q^{2(j-1)}\right]^2, \quad (4.1)$$

where P_{PD}, ν_2, …, ν_{2M} are (M+1) adjustable parameters. We allowed M to range from 1 to 4, and in each case we looked for the parameter values which minimise the corresponding χ^2–expression, with the further constraint that

$$\left|I_{obs}(q_k)-Vq_k^4\left[\sum_{j=2}^{M}(-1)^j\nu_{2j}q_k^{2(j-1)}\right]^2\right|<\varepsilon_k$$

at each observed q_k value, ε_k denoting the corresponding error on the intensity value observed. This condition ensures that $I_D(q)$ turns out to be positive within experimental errors. In Fig.5, the dotted, short-dash, long-dash and continuous lines represent the result of the best-fits for M=1,2,3 and 4 respectively. Comparing the χ^2 value with the number of the freedom degrees (i.e. the number of fitted points minus the parameter number), the best-fits for the samples at the temperatures of 40, 50, 60, 75, 90 and 100°C are satisfactory with M=2. For samples at 120 and 150°C, M must be taken as equal to 3 and 4. Figures 2–6 of [14] show the final Porod plots. For greater homogeneity, Table I reports the nu-

Table I. *Best-fitted parameter values*

T°C	P_{PD}	$\sqrt{V}\nu_2$	$\sqrt{V}\nu_4$
40	132	12	–2.4
50	176	12	–2.2
60	184	13	–2.5
75	197	13	–2.4
90	201	17	–3.5
100	279	19	–3.6
120	166	25	–5.3
150	988	40	–7.9

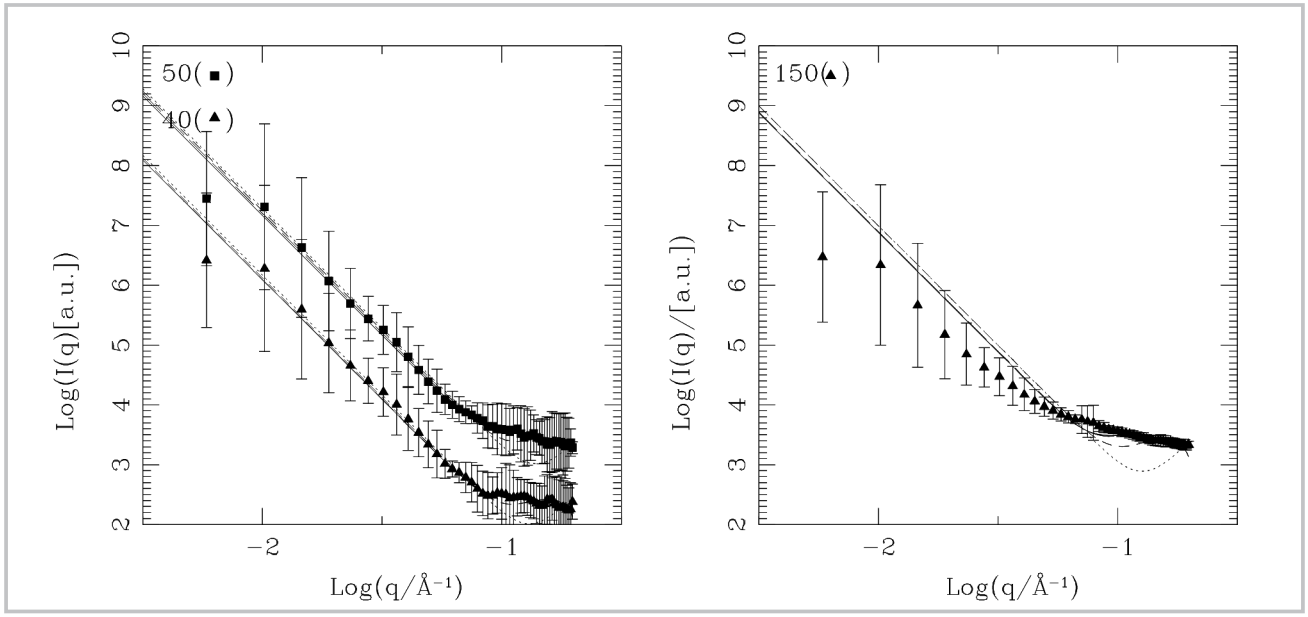

Figure 5. *Log-log plots of the SAS intensities for the best (left) and worst case (right). The dotted, the short dash, the long-dash and the continuous lines refer to Eq. (4.1) with M = 1, 2, 3 and 4, respectively. Note that the best-fitted q range is [0.05-0.2]Å^{-1}.*

merical values of the best-fitted parameters obtained with M=2. The first column reports the temperature of each sample, columns 2, 3 and 4 the values of P_{PD}, $\sqrt{V}\nu_2$ and $\sqrt{V}\nu_4$, as specified by the column headings.

Since the analysed intensities are known in relative units [u], the units of P_{PD}, $\sqrt{V}\nu_2$ and $\sqrt{V}\nu_4$ respectively are $nm^{-4}[u]$, $nm^2[u]^{1/2}$, $nm^4[u]^{1/2}$. The statistical relative errors [13] for P_{PD}, ν_2 and ν_4 are smaller than 10%, 1% and 2% respectively. From the comparison of the values reported in table I with those obtained from the best-fits with M=4, the variations for P_{PD}, ν_2 and ν_4 are found to be smaller than 15%, 25% and 40%. Thus it appears more sound to consider the latter values as the uncertainties of the values reported in table I.

The table reports the parameter values resulting from the best-fits of Eq. (4.1) to the SAS X-ray intensities relevant to a semi-halato-telechelic polymer sample at the temperatures reported in the first column. The values of the Porod coefficient and of the second and fourth moment of the microscopic fluctuation density are reported in columns 2, 3 and 4 respectively. The best-fitted q-range is [0.5–2]nm^{-1}.

For the discussion of the results reported in the table we refer to [14]. Consider now the square root of the ratio $|\nu_4/\nu_2|$. From Eq. (2.15) one obtains

$$|\nu_4/\nu_2|^{1/2} = \left[(1/5)\left|\int r^4 \nu_D(r)dV \int r^2 \nu_D(r)dV\right|\right]^{1/2}$$

which has length dimension. Similar to Guinier's law [20], one can consider

$$\ell_{mfl} = 5^{1/2}|\nu_4/\nu_2|^{1/2}$$

as the typical scale-length on which the density microscopic fluctuation varies. From the values of Table I, one finds that $\ell_{mfl} \approx 1\,nm$, a value which is physically quite reasonable. One concludes that, as the sample temperature increases, the density microscopic fluctuation increases in amplitude but the length scale on which it changes remains essentially the same.

5. Conclusion

The main conclusion of the paper is that the background contribution to isotropic SAS intensities can be described by the analytic expression Eq.5.1.
where
$\nu_{2\ell}$ is 2ℓth the moment of the scattering density fluctuation. We refer to the end of Section 2 for the discussion of the assumptions ensuring the validity of Eq. (5.1).

We also remark that: (a) the existence of a Porod region, understood in our analysis, is a condition not met in the case of fractal samples, even though a background term is often considered in best-fitting the data to a power-law behaviour in these cases also (see, e.g. [17]). Recalling that fractal samples are often described as a collection of homogeneous monomers arranged with fractal geometry [18], it appears evident that Eq. (1.8) also applies to these systems because the monomers are only approximately homogeneous. By the same discussion which led us to write Eqs. (1.4), (1.5) and (1.6), one concludes that $I_{bck}(q)$ is still given by Eq. (4.1), while $I_D(q)$ takes now the power-law form F/q^α; (b) the case of negative deviations from Porod's law can also be treated by a slight modification of the procedure expounded above. In fact, by following Ruland's suggestion [7], one substitutes $\eta_D(r)$ with $\int \eta_D(r_1)\exp\left(-\left(|r_1 - r|/\sigma\right)^2\right)dV_1$ in Eq. (2.6), where σ is proportional to the thickness of the interphase regions. This implies that the SAS intensities observed have to be best-fitted to $\left[P_{PD}\exp\left(-\sigma^2 q^2/2\right)/q^4 + I_{bck}(q)\right]$ instead of $\left[P_{PD}/q^4 + I_{bck}(q)\right]$ while $I_{bck}(q)$ is still given by Eq. (4.1); and (c) the aforesaid background subtraction procedure can easily be extended to the case of slit-collimated intensities using the relations reported in sect. 3.4 of [27].

Our concluding remark is the recommendation to convert the best-fitted parameters' values, which are always determined when Porod's law is applied, into the moments of the density microscopic fluctuation, since these can yield useful information on the latter quantity.

❑

Equation 5.1

$$I_{bck}(q) \approx I_{mfl}(q) \approx Vq^4\left[\nu_2 - \nu_4 q^2 + \nu_6 q^4 + \ldots\right]^2, \qquad (5.1)$$

Acknowledgments

I warmly thank Dr. Roger Sobry for having allowed me to present here some original results obtained during our fruitful and friendly collaboration on this issue.

References

1. P. Debye, H.R. Anderson and H. Brumberger, J. Appl. Phys. 28, 679, (1957).
2. S. Ciccariello, in preparation, (2002).
3. S. Ciccariello, J. Goodisman and H. Brumberger, J. Appl. Cryst. 21, 117, (1988).
4. G. Porod, Kolloid-Z., 124, 83, (1951); ibid. 125, 51, (1951), and ibid. 125, 109, (1951).
5. S. Ciccariello, J. Appl. Cryst. 24, 509, (1991).
6. V. Luzzati, J. Witz and A. Nicolaie, J. Mol. Biol. 3, 367, (1961).
7. W. Ruland, J. Appl. Cryst. 4, 70, (1971).
8. C. G. Vonk, J. Appl. Cryst. 6, 81, (1973).
9. R. Bonart and E. H. Müller, J. Macromol. Sci. Phys. B 10, 177, (1974).
10. J. Rathje and W. Ruland, Colloid. Polym. Sci. 254, 358, (1976).
11. J. T. Koberstein, B. Morra and R. Stein, J. Appl. Cryst. 13, 34, (1980).
12. R.-J.Roe, J. Appl. Cryst. 15, 182, (1982).
13. L. Lyons, A practical guide to data analysis for physical science students, (Cambridge University Press: Cambridge), (1991).
14. R. Sobry and S. Ciccariello, J. Appl. Cryst. 35, in the press, (2002).
15. W. Ruland, Macromolecules 20, 87, (1987).
16. A.N. Semenov, Macromolecules 27, 2732, (1994).
17. H.D. Bale and P.W. Schmidt, Phys. Rev. Lett 53, 596, (1984).
18. T. Freltoft, J.K. Kjems and S.K. Sinha, Phys. Rev. B 33, 269, (1986).
19. P. Debye and A. M. Bueche, J. Appl. Phys. 20, 518, (1949).
20. A. Guinier and G. Fournet, Small-angle scattering of X-rays, (Wiley: New York), (1955).
21. W. Wiegand and W. Ruland, Prog. Colloid Polym. Sci. 66, 355, (1979).
22. S. Ciccariello, J-M. Schneider, B. Schönfeld and G. Kostorz, J. Appl. Cryst. 35, in the press, (2002).
23. J.P. Hansen and I.R. McDonald, Theory of simple liquids, (Academic Press: London), (1976).
24. M.S. Wertheim, J. Math. Phys. 5, 643, (1964).
25. J.-F. Gohy, P. Vanhoorne and R. Jérôme, Macromolecules 29, 3376, (1996).
26. R. Sobry, G. Van den Bossche, F. Fontaine, J.-F. Gohy and R. Jérôme, J.Appl. Cryst. 30, 1075, (1997).
27. S. Ciccariello and R. Sobry, J. Appl. Cryst. 32, 579, (1999).

❑ ***Received 14.01.2003, Revieved 05.05.2003***